

Negative Energy and Angular Momentum Modes of Thin Accretion Disks

L. Zhang* R.V.E. Lovelace†

Abstract

This work derives the linearized equations of motion, the Lagrangian density, the Hamiltonian density, and the canonical angular momentum density for general perturbations [$\propto \exp(im\phi)$ with $m = 0, \pm 1, \dots$] of a geometrically thin self-gravitating, homentropic fluid disk including the pressure. The theory is applied to “eccentric,” $m = \pm 1$ perturbations of a geometrically thin Keplerian disk. We find $m = 1$ modes at low frequencies relative to the Keplerian frequency. Further, it is shown that these modes can have negative energy and negative angular momentum. The radial propagation of these low frequency $m = 1$ modes can transport angular momentum away from the inner region of a disk and thus increase the rate of mass accretion. Depending on the radial boundary conditions there can be discrete low-frequency, negative-energy, $m = 1$ modes.

key words: accretion, accretion disks—instabilities— galaxies: kinematics and dynamics

1 Introduction

Problems of long standing interest concern the linear modes and instabilities of accretion disks and the disks of spiral galaxies (for example, Kato, Fukue, & Mineshige 1998; Binney & Tremaine 1987). Interest in unstable modes in accretion disks has been stimulated by recent observations of quasi-periodic oscillations (QPOs) in accreting neutron stars and black hole candidates in binary systems (see review by van der Klis 2000). On a larger scale, recent observations of disk galaxies reveal that about 30% of the disks are “lopsided” (Baldwin, Lynden-Bell, & Sancisi 1980; Rix & Zaritsky 1995; Kornreich, Haynes, & Lovelace 1998). In some cases the lopsidedness may be dynamical in origin and an indication of an unstable one-armed trailing spiral wave (Lovelace, Zhang, Kornreich, & Haynes 1999; hereafter LZKH). Hybrid, N-body/hydrodynamic simulations of impulsively perturbed disk galaxies show long-lived trailing spiral features (Zeltwanger *et al.* 2000; Kornreich *et al.* 2002).

*Pennsylvania State University, University Park, PA 16802; LXZ1@psu.edu

†Department of Astronomy, Cornell University, Ithaca, NY 14853; RVL1@cornell.edu

In previous work we derived equations of motion, a Lagrangian, Hamiltonian, and canonical angular momentum for the eccentric perturbations [$\propto \exp(\pm i\phi)$] of a thin self-gravitating disk of a galaxy consisting of a large number of rings (LZKH). This work utilized a Lagrangian description of the perturbation. The present work generalizes LZKH by deriving equations of motion, a Lagrangian density, Hamiltonian density, and canonical angular momentum density for general perturbations [$\propto \exp(im\phi)$ with $m = 0, \pm 1, \dots$] of a self-gravitating fluid disk including the pressure. The theory allows the calculation of the energy and angular momentum of the different modes and identification of modes with *negative energy* and/or *negative angular momentum*. The negative energy modes can become unstable in the presence of dissipation. Negative energy modes are important in plasma physics (Coppi, Rosenbluth, & Sudan 1969), in Rossby r-mode oscillations of rapidly rotating neutron stars which are made unstable by gravitational radiation (Andersson 1998; Schenk *et al.* 2002), and for short wavelength modes in the shearing sheet model of modes of disks (Goodman, Narayan, & Goldreich 1987). We apply our theory to the “eccentric,” $m = 1$ perturbations of a geometrically thin Keplerian disk. We find $m = 1$ modes with frequencies much less than the Keplerian frequency. These modes can have negative energy and negative angular momentum. The radial propagation of such a mode may act to remove angular momentum from the inner region of a disk. Earlier, Nowak and Wagoner (1991, 1992) analyzed the modes of non-self-gravitating disks using a Lagrangian description of the perturbation. The important role of $m = 1$ modes for accretion disk angular momentum transport has been discussed by Fridman *et al.* (2003). Adams, Ruden, and Shu (1989) studied the growth of global gravitational instabilities in star/disk systems and found modes which grow on a nearly dynamical time scale. Shu *et al.* (1990) presented an analytical description of the corresponding modal mechanisms. Tremaine (2001) analyzed slow modes using softened gravity and found these modes to be stable.

In §2 we derive the linearized equations of motion and obtain the Lagrangian density. From this the Hamiltonian density and canonical angular momentum density are derived in the usual way. In §3 we introduce a representation for the perturbation amplitudes in terms of complex quantities. In §4 the WKBJ approximation is introduced for the radial dependence of the perturbations, and the results of the present approach are contrasted with the standard analysis. In §5 we consider the inner region of a low mass disk around a black hole and show that one of the $m = 1$ modes has a very low frequency (compared with the rotational frequency). This mode is shown to have negative energy which means that it may be made unstable by dissipation. In §6 we give conclusions of this work.

2 Theory

We use an inertial cylindrical (r, ϕ, z) coordinate system and assume that the disk is geometrically thin with half-thickness $h \ll r$. Further, we consider

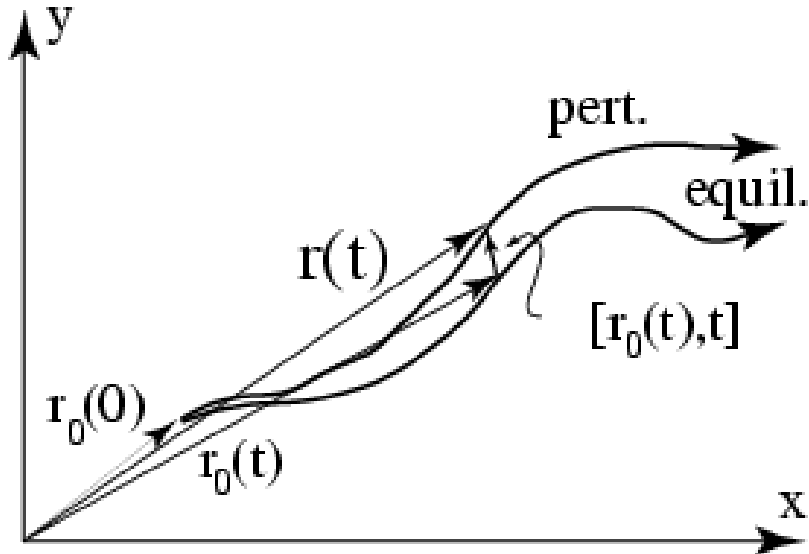


Figure 1: Diagram illustrating equation (1), where “equil.” indicates the equilibrium path of a fluid element and “pert.” indicates the perturbed path. See Frieman & Rotenberg (1960).

conditions where the accretion speed $-v_r \ll v_\phi$. We use a Lagrangian representation for the perturbation as developed by Frieman and Rotenberg (1960) and Lynden-Bell and Ostriker (1967) and as applied to a system of rings representing a self-gravitating disk (LZKH; Lovelace 1998). The position vector \mathbf{r} of a fluid element which at $t = 0$ was at \mathbf{r}_0 is given by

$$\mathbf{r}(t) = \mathbf{r}_0(t) + \boldsymbol{\xi}(\mathbf{r}_0, t) . \quad (1)$$

That is, $\mathbf{r}_0(t)$ is the unperturbed and $\mathbf{r}(t)$ the perturbed orbit of a fluid element as sketched in Figure 1.

Further, the perturbations are assumed to consist of small in-plane displacements of the disk matter,

$$\boldsymbol{\xi} = \xi_r \hat{\mathbf{r}} + \xi_\phi \hat{\boldsymbol{\phi}} . \quad (2)$$

The ξ_r and ξ_ϕ are proportional to $\exp(im\phi)$ with $m = 0, 1, 2, \dots$ the azimuthal mode number. (The negative values of m are redundant.)

From equation (1), we have $\mathbf{v}(\mathbf{r}, t) = \mathbf{v}_0(\mathbf{r}_0, t) + \partial\boldsymbol{\xi}/\partial t + (\mathbf{v} \cdot \nabla)\boldsymbol{\xi}$. The Eulerian velocity perturbation is $\delta\mathbf{v}(\mathbf{r}, t) \equiv \mathbf{v}(\mathbf{r}, t) - \mathbf{v}_0(\mathbf{r}, t)$. Therefore,

$$\delta\mathbf{v}(\mathbf{r}, t) = \frac{\partial\boldsymbol{\xi}}{\partial t} + (\mathbf{v} \cdot \nabla)\boldsymbol{\xi} - (\boldsymbol{\xi} \cdot \nabla)\mathbf{v} . \quad (3)$$

The components of this equation are

$$\begin{aligned}\delta v_r &= \mathcal{D} \xi_r , \\ \delta v_\phi &= \mathcal{D} \xi_\phi - r\Omega' \xi_r ,\end{aligned}\tag{4}$$

where

$$\mathcal{D} \equiv \frac{\partial}{\partial t} + \Omega(r) \frac{\partial}{\partial \phi} ,$$

with $\Omega(r)$ the angular rotation rate of the equilibrium disk and $\Omega' \equiv d\Omega/dr$.

The equation of motion is

$$\frac{d \delta \mathbf{v}}{dt} = \delta \mathbf{F} = -\frac{1}{\Sigma} \nabla \delta P + \frac{\delta \Sigma}{\Sigma^2} \nabla P - \nabla \delta \Phi ,\tag{5}$$

where $\delta \mathbf{F}$ is the perturbation force per unit mass, $\delta \Phi$ is the perturbation of the gravitational potential, Σ is the disk's surface mass density, and P is the vertically integrated pressure in the disk. For simplicity we consider a homentropic disk where $P = \text{const } \Sigma^\Gamma$. Under this condition, $\delta \mathbf{F} = -\nabla(\delta P/\Sigma) - \nabla \delta \Phi$.

We have

$$\frac{d \delta \mathbf{v}}{dt} = \frac{\partial \delta \mathbf{v}}{\partial t} + (\mathbf{v} \cdot \nabla) \delta \mathbf{v} + (\delta \mathbf{v} \cdot \nabla) \mathbf{v} .\tag{6}$$

The components of equation (6) give

$$\begin{aligned}\left(\frac{d \delta \mathbf{v}}{dt}\right)_r &= \mathcal{D} \delta v_r - 2\Omega \delta v_\phi , \\ &= (\mathcal{D}^2 + 2\Omega r \Omega') \xi_r - 2\Omega \mathcal{D} \xi_\phi , \\ \left(\frac{d \delta \mathbf{v}}{dt}\right)_\phi &= \mathcal{D} \delta v_\phi + (\kappa_r^2/2\Omega) \delta v_r , \\ &= \mathcal{D}^2 \xi_\phi + 2\Omega \mathcal{D} \xi_r ,\end{aligned}\tag{7}$$

where $\kappa_r^2 \equiv (1/r^3)d(r^4\Omega^2)/dr$ is the radial epicyclic frequency (squared). For a low mass, geometrically thin Keplerian disk, $\kappa_r^2 = \Omega^2 + \mathcal{O}(c_s^2/r^2) \approx \Omega^2$. More generally, for $\Omega \propto 1/r^q$, $\kappa_r^2 = 2(2-q)\Omega^2$. For a Keplerian disk, $q = 3/2$; for a spiral galaxy with a flat rotation curve, $q = 1$; and for a rigidly rotating disk, for example, the inner region of a spiral galaxy, $q = 0$.

For $\delta \mathbf{F} = 0$, equations (7) with $\xi_r, \xi_\phi \propto \exp(im\phi - i\omega t)$ can be solved to give four roots: two have $\omega - m\Omega = 0$ and $\xi_r = 0, \xi_\phi \neq 0$, and two have $\omega - m\Omega = \pm \kappa_r$. For the second pair of modes, $\mathcal{R}e(\xi_r) = a \cos(\kappa_r t)$ and $\mathcal{R}e(\xi_\phi) = -(2\Omega/\kappa) a \sin(\kappa_r t)$, where $a = \text{const.}$ and $\mathcal{R}e$ indicates the real part; the fluid particle moves along a retrograde ellipse which is elongated in the azimuthal direction since $\kappa_r < 2\Omega$ for most conditions (Binney & Tremaine 1987, p. 132). For a rigidly rotating disk, $2\Omega/\kappa_r = 1$ so that the ellipse is a circle.

The perturbation of the surface mass density of the disk obeys

$$\frac{\partial \delta \Sigma}{\partial t} + \nabla \cdot (\Sigma \delta \mathbf{v} + \delta \Sigma \mathbf{v}) = 0 ,$$

where $\Sigma(r)$ is the surface density of the equilibrium disk. Because $\nabla \cdot (\Sigma \mathbf{v}) = 0$, this equation implies

$$\delta\Sigma = -\nabla \cdot (\Sigma \boldsymbol{\xi}) . \quad (8)$$

The perturbation of the gravitational potential is given by

$$\delta\Phi(\mathbf{r}, t) = -G \int d^2r' \frac{\delta\Sigma(\mathbf{r}', t)}{|\mathbf{r} - \mathbf{r}'|} , \quad (9)$$

where the integration is over the surface area of the disk, and G is the gravitational constant.

2.1 Perturbation Amplitudes

We can write in general

$$\begin{aligned} \xi_r &= \epsilon_x \cos(m\phi) + \epsilon_y \sin(m\phi) , \\ \xi_\phi &= -\delta_x \sin(m\phi) + \delta_y \cos(m\phi) , \end{aligned} \quad (10)$$

where $\epsilon_{x,y}(r, t)$ and $\delta_{x,y}(r, t)$ are the *displacement amplitudes* for the ‘ring’ of the disk at radius r . For $m = 1$, $\epsilon_{x,y}$ represents the shift of the ring’s center, and $\delta_{x,y}$ represents in general both the shift of the ring’s center *and* the azimuthal displacement of the ring matter (see LZKH).

2.2 Equations of Motion

From equations (5) - (7) and (10), we obtain the disk equations of motion,

$$\begin{aligned} \ddot{\epsilon}_x + 2m\Omega\dot{\epsilon}_y - m^2\tilde{\Omega}^2\epsilon_x - 2\Omega(\dot{\delta}_y - m\Omega\delta_x) &= \delta F_r^C , \\ \ddot{\epsilon}_y - 2m\Omega\dot{\epsilon}_x - m^2\tilde{\Omega}^2\epsilon_y + 2\Omega(\dot{\delta}_x + m\Omega\delta_y) &= \delta F_r^S , \\ \ddot{\delta}_x + 2m\Omega\dot{\delta}_y - m^2\Omega^2\delta_x - 2\Omega(\dot{\epsilon}_y - m\Omega\epsilon_x) &= -\delta F_\phi^S , \\ \ddot{\delta}_y - 2m\Omega\dot{\delta}_x - m^2\Omega^2\delta_y + 2\Omega(\dot{\epsilon}_x + m\Omega\epsilon_y) &= \delta F_\phi^C , \end{aligned} \quad (11)$$

where $\dot{\epsilon}_x \equiv \partial\epsilon_x(r, t)/\partial t$, etc. Here,

$$\tilde{\Omega}^2 \equiv \Omega^2 - 2\Omega r \Omega' / m^2 ,$$

and

$$\delta F_\alpha^{C,S} \equiv \oint \frac{d\phi}{\pi} [\cos(m\phi), \sin(m\phi)] \delta F_\alpha ,$$

with the S, C superscripts denoting the sine and cosine components, and $\alpha = r, \phi$.

The force per unit mass

$$\delta F_\alpha = -\nabla \frac{\delta P}{\Sigma} - \nabla \delta\Phi = \nabla \left[\frac{c_s^2 \nabla \cdot (\Sigma \boldsymbol{\xi})}{\Sigma} \right] - \nabla \delta\Phi , \quad (12)$$

with $\alpha = r, \phi$, and $c_s^2 = dP/d\Sigma$ is the effective sound speed (squared). The pressure force on the right-hand side of equation (12) gives

$$\begin{aligned}
\delta F_r^{Cp} &= D[c_s^2 D_\star(\Sigma\epsilon_x)/\Sigma] - D(c_s^2 m\delta_x/r) , \\
\delta F_r^{Sp} &= D[c_s^2 D_\star(\Sigma\epsilon_y)/\Sigma] - D(c_s^2 m\delta_y/r) , \\
-\delta F_\phi^{Sp} &= [mc_s^2/(r\Sigma)]D_\star(\Sigma\epsilon_x) - c_s^2 m^2\delta_x/r^2 , \\
\delta F_\phi^{Cp} &= [mc_s^2/(r\Sigma)]D_\star(\Sigma\epsilon_y) - c_s^2 m^2\delta_y/r^2 ,
\end{aligned} \tag{13}$$

where $D(\cdot) \equiv \partial(\cdot)/\partial r$ and $D_\star(\cdot) \equiv (1/r)\partial(r \cdot)/\partial r$.

The gravitational force gives

$$\begin{aligned}
\delta F_r^{Cg} &= -\frac{\partial}{\partial r} G \int d^2 r' \mathcal{K}_m R'_x , \\
\delta F_r^{Sg} &= -\frac{\partial}{\partial r} G \int d^2 r' \mathcal{K}_m R'_y , \\
-\delta F_\phi^{Sg} &= -\frac{m}{r} G \int d^2 r' \mathcal{K}_m R'_x , \\
\delta F_\phi^{Cg} &= -\frac{m}{r} G \int d^2 r' \mathcal{K}_m R'_y ,
\end{aligned} \tag{14}$$

where $d^2 r' = 2\pi r' dr'$, $R_j = R_j(r', t)$,

$$R_j(r) \equiv D_\star(\Sigma\epsilon_j) - m\Sigma\delta_j/r \tag{15}$$

for $j = x, y$, and

$$\mathcal{K}_m(r, r') \equiv \frac{1}{2\pi} \oint \frac{d\Psi \cos(m\Psi)}{\sqrt{r^2 + (r')^2 - 2rr' \cos(\Psi)}} . \tag{16}$$

We can express this as

$$\mathcal{K}_m(r, r') = \frac{(-2)^m}{(2m-1)!!} \frac{P_{-1/2}^m(z)}{\sqrt{|r^2 - (r')^2|}} ,$$

where $z \equiv [r^2 + (r')^2]/|r^2 - (r')^2|$, $(-1)!! = 1$, and P_ν^m is the usual associated Legendre function.

2.3 Lagrangian

The Lagrangian which gives the above equations of motion is

$$L = \int d^2 r \mathcal{L} = 2\pi \int r dr \mathcal{L} , \tag{17}$$

where $\mathcal{L} = \mathcal{L}_0 + \mathcal{L}_1 + \mathcal{L}_2 + \mathcal{L}_3$ is the Lagrangian density with

$$\mathcal{L}_0 = \frac{\Sigma}{2} \left[\dot{\epsilon}^2 + \dot{\delta}^2 + m^2 \tilde{\Omega}^2 \epsilon^2 + m^2 \Omega^2 \delta^2 - 4m\Omega^2 \epsilon \cdot \delta \right] ,$$

$$\mathcal{L}_1 = -\Sigma\Omega \left[m\boldsymbol{\epsilon} \times \dot{\boldsymbol{\epsilon}} + m\boldsymbol{\delta} \times \dot{\boldsymbol{\delta}} - \boldsymbol{\delta} \times \dot{\boldsymbol{\epsilon}} - \boldsymbol{\epsilon} \times \dot{\boldsymbol{\delta}} \right] \cdot \hat{\mathbf{z}} ,$$

$$\begin{aligned} \mathcal{L}_2 &= -\frac{c_s^2}{2\Sigma} [\nabla \cdot (\Sigma\boldsymbol{\xi})]^2 \\ &= -\frac{1}{2}\Sigma c_s^2 \left(\mathbf{Q} - \frac{m\boldsymbol{\delta}}{r} \right)^2 , \end{aligned}$$

$$\mathcal{L}_3 = \frac{G}{2}\Sigma \left(\mathbf{Q} - \frac{m\boldsymbol{\delta}}{r} \right) \cdot \int d^2r' \mathcal{K}_m(r, r') \Sigma' \left(\mathbf{Q}' - \frac{m\boldsymbol{\delta}'}{r'} \right) . \quad (18)$$

Here, $\boldsymbol{\epsilon} \equiv \epsilon_x \hat{\mathbf{x}} + \epsilon_y \hat{\mathbf{y}}$, $\boldsymbol{\delta} \equiv \delta_x \hat{\mathbf{x}} + \delta_y \hat{\mathbf{y}}$, $Q_j(r) \equiv D_\star(\Sigma\epsilon_j)/\Sigma$ ($j = x, y$), $\mathbf{Q} \equiv Q_x \hat{\mathbf{x}} + Q_y \hat{\mathbf{y}}$, and $\Sigma' = \Sigma(r')$.

The Lagrangian density is $\mathcal{L} = \mathcal{L}[\boldsymbol{\epsilon}, \boldsymbol{\delta}, \dot{\boldsymbol{\epsilon}}, \dot{\boldsymbol{\delta}}, \mathbf{Q}]$. In terms of functional derivatives, the equations of motion are

$$\begin{aligned} \frac{\partial}{\partial t} \frac{\delta L}{\delta \dot{\epsilon}_j} &= \frac{\delta L}{\delta \epsilon_j} - \Sigma \frac{\partial}{\partial r} \left(\frac{1}{\Sigma} \frac{\delta L}{\delta Q_j} \right) , \\ \frac{\partial}{\partial t} \frac{\delta L}{\delta \dot{\delta}_j} &= \frac{\delta L}{\delta \delta_j} , \end{aligned} \quad (19)$$

(see for example Goldstein 1950, ch. 11). For the contribution from \mathcal{L}_3 , $\delta L_3/\delta \mathbf{Q} = G\Sigma \int d^2r' \mathcal{K}_m \Sigma' (\mathbf{Q}' - m\boldsymbol{\delta}'/r')$ and $\delta L_3/\delta \boldsymbol{\delta} = -G\Sigma(m/r) \int d^2r' \mathcal{K}_m \Sigma' (\mathbf{Q}' - m\boldsymbol{\delta}'/r')$.

2.4 Hamiltonian

The Hamiltonian density is

$$\mathcal{H} = \dot{\boldsymbol{\epsilon}} \cdot \frac{\partial \mathcal{L}}{\partial \dot{\boldsymbol{\epsilon}}} + \dot{\boldsymbol{\delta}} \cdot \frac{\partial \mathcal{L}}{\partial \dot{\boldsymbol{\delta}}} - \mathcal{L} . \quad (20)$$

The time derivative of this equation gives

$$\frac{\partial \mathcal{H}}{\partial t} + \frac{1}{r} \frac{\partial}{\partial r} (r \mathcal{F}_{Er}) = 0 , \quad \mathcal{F}_{Er} \equiv \dot{\boldsymbol{\epsilon}} \cdot \frac{\partial \mathcal{L}}{\partial \mathbf{Q}} , \quad (21)$$

where \mathcal{F}_{Er} is the radial energy flux-density. The explicit Hamiltonian density is

$$\begin{aligned} \mathcal{H} &= \frac{\Sigma}{2} \left(\dot{\boldsymbol{\epsilon}}^2 + \dot{\boldsymbol{\delta}}^2 - m^2 \tilde{\Omega}^2 \boldsymbol{\epsilon}^2 - m^2 \Omega^2 \boldsymbol{\delta}^2 + 4m\Omega^2 \boldsymbol{\epsilon} \cdot \boldsymbol{\delta} \right) \\ &+ \frac{1}{2}\Sigma c_s^2 \left(\mathbf{Q} - \frac{m\boldsymbol{\delta}}{r} \right)^2 \\ &- \frac{G}{2}\Sigma \left(\mathbf{Q} - \frac{m\boldsymbol{\delta}}{r} \right) \cdot \int d^2r' \mathcal{K}_m \Sigma' \left(\mathbf{Q}' - \frac{m\boldsymbol{\delta}'}{r'} \right) \end{aligned} \quad (22)$$

in terms of the Lagrangian variables. Assuming vanishing energy fluxes through the inner and outer radii of the disk, we have

$$H \equiv \int d^2r \mathcal{H} , \quad \text{with} \quad \frac{dH}{dt} = 0 , \quad (23)$$

where $H = E$ is the energy of the perturbation.

2.5 Canonical Angular Momentum

We can make a canonical transformation from rectangular to polar coordinates, $(\epsilon_x, \epsilon_y) \rightarrow (\epsilon, \varphi)$, $(\delta_x, \delta_y) \rightarrow (\delta, \psi)$ to obtain the Lagrangian as $\mathcal{L} = \mathcal{L}(\epsilon, \delta, \varphi, \psi, \dot{\epsilon}, \dot{\delta}, \dot{\varphi}, \dot{\psi}, D_\star(\Sigma\epsilon)/\Sigma, \partial\varphi/\partial r)$. Note for example that $\dot{\epsilon}^2 \rightarrow \dot{\epsilon}^2 + \epsilon^2 \dot{\varphi}^2$. We then find that \mathcal{L} is invariant under the simultaneous changes $\varphi \rightarrow \varphi + \theta$, $\psi \rightarrow \psi + \theta$. Therefore, it is useful to make a further canonical transformation, $[\varphi, \psi] \rightarrow [\alpha = (\varphi + \psi)/2, \beta = \varphi - \psi]$, which gives $\partial\mathcal{L}/\partial\alpha = 0$. Defining the canonical angular momentum density as

$$\mathcal{P}_\phi \equiv \frac{\partial\mathcal{L}}{\partial\dot{\alpha}} ,$$

we obtain

$$\frac{\partial\mathcal{P}_\phi}{\partial t} + \frac{1}{r} \frac{\partial}{\partial r} (r \mathcal{F}_{\mathcal{P}_r}) = 0 , \quad \mathcal{F}_{\mathcal{P}_r} \equiv \frac{\partial\mathcal{L}}{\partial(\partial\alpha/\partial r)} , \quad (24)$$

where $\mathcal{F}_{\mathcal{P}_r}$ is the radial flux-density of angular momentum. Assuming vanishing angular momentum fluxes through the inner and outer radii of the disk, we have

$$P_\phi = \int d^2r \mathcal{P}_\phi , \quad \text{with} \quad \frac{dP_\phi}{dt} = 0 , \quad (25)$$

where P_ϕ is the canonical angular momentum of the perturbation. From equation (20) we find

$$\mathcal{P}_\phi = \Sigma \left[\epsilon^2 (\dot{\varphi} - m\Omega) + \delta^2 (\dot{\psi} - m\Omega) + 2\Omega\epsilon\delta \cos(\varphi - \psi) \right] , \quad (26)$$

where the last term can also be written as $2\Sigma\Omega\epsilon \cdot \delta$.

3 Complex Displacement Amplitudes

It is useful for later work to introduce the complex displacement amplitudes,

$$\begin{aligned} \mathcal{E} &\equiv \epsilon_x - i\epsilon_y = \epsilon(r, t) \exp [-i\varphi(r, t)] , \\ \Delta &\equiv \delta_x - i\delta_y = \delta(r, t) \exp [-i\psi(r, t)] , \end{aligned} \quad (27)$$

(LZKH). Here, ϵ and δ are clearly non-negative, and the angles φ and ψ are the line-of-nodes angles for the \mathcal{E} and Δ components of the perturbation. In terms of these complex amplitudes, equations (11) can be combined to give

$$\ddot{\mathcal{E}} + 2im\Omega\dot{\mathcal{E}} - m^2\tilde{\Omega}^2\mathcal{E} - 2i\Omega\dot{\Delta} + 2m\Omega^2\Delta = \delta F_{\mathcal{E}} ,$$

$$\ddot{\Delta} + 2im\Omega\dot{\Delta} - m^2\Omega^2\Delta - 2i\Omega\dot{\mathcal{E}} + 2m\Omega^2\mathcal{E} = \delta F_{\Delta} , \quad (28)$$

where $\delta F_{\mathcal{E}} \equiv \delta F_r^C - i\delta F_r^S$ and $\delta F_{\Delta} \equiv -\delta F_{\phi}^S - i\delta F_{\phi}^C$.

4 WKBJ Approximation

For perturbations with short radial wavelengths $\lambda_r = 2\pi/|k_r|$, the WKBJ approximation is useful. That is, for $h < \lambda_r/(2\pi) < r$, we can take \mathcal{E} , $\Delta \sim \exp[i \int^r dr' k_r(r')]$ in equation (18). The radial derivatives can be approximated as for example $D_*(\Sigma\mathcal{E}) \approx ik_r\Sigma\mathcal{E}$. The azimuthal wavenumber $k_{\phi} \equiv m/r$ is assumed to be less than or of the order of $|k_r|$ which corresponds to $0 \leq m < r/h$. Note that the radial wavenumber k_r may be > 0 or < 0 . For $m \geq 1$, $k_r > 0$ corresponds to a trailing spiral wave and $k_r < 0$ to a leading spiral wave.

With the WKBJ approximation, the pressure force becomes

$$\begin{aligned} \delta F_{\mathcal{E}}^p &= -k_r^2 c_s^2 \mathcal{E} - ik_r k_{\phi} c_s^2 \Delta , \\ \delta F_{\Delta}^p &= -k_{\phi}^2 c_s^2 \Delta + ik_r k_{\phi} c_s^2 \mathcal{E} . \end{aligned} \quad (29)$$

The gravitational force is

$$\begin{aligned} \delta F_{\mathcal{E}}^g &= 2\pi G\Sigma(k_r^2 \mathcal{E} + ik_r k_{\phi} \Delta)/k , \\ \delta F_{\Delta}^g &= 2\pi G\Sigma(k_{\phi}^2 \Delta - ik_r k_{\phi} \mathcal{E})/k , \end{aligned} \quad (30)$$

where $k \equiv (k_r^2 + k_{\phi}^2)^{1/2}$.

In terms of \mathcal{E} and Δ , the Hamiltonian density in the WKBJ approximation becomes

$$\begin{aligned} \mathcal{H} &= \frac{\Sigma}{2} \left(|\dot{\mathcal{E}}|^2 + |\dot{\Delta}|^2 - (m^2\Omega^2 - 2\Omega r\Omega') |\mathcal{E}|^2 \right. \\ &\quad \left. - m^2\Omega^2 |\Delta|^2 + 4m\Omega^2 \mathcal{R}e(\mathcal{E}\Delta^*) \right) \\ &\quad + \frac{\Sigma u^2}{2} |ik_r \mathcal{E} - k_{\phi} \Delta|^2 , \end{aligned} \quad (31)$$

where $u^2 \equiv c_s^2 - 2\pi G\Sigma/k$, $\mathcal{R}e(\cdot)$ indicates the real part, and $(\cdot)^*$ the complex conjugate. The radial energy flux-density is

$$\begin{aligned} \mathcal{F}_{Er} &= -\Sigma u^2 \dot{\mathcal{E}} \cdot (\mathbf{Q} - k_{\phi} \boldsymbol{\delta}) \\ &= -\Sigma u^2 \mathcal{R}e[\dot{\mathcal{E}}^* (ik_r \mathcal{E} - k_{\phi} \Delta)] , \end{aligned} \quad (32)$$

from equation (23).

Similarly, the canonical angular momentum density can be written as

$$\begin{aligned} \mathcal{P}_{\phi} &= \Sigma \left\{ \mathcal{I}m[\mathcal{E}(\dot{\mathcal{E}}^* - im\Omega\mathcal{E}^*)] + \mathcal{I}m[\Delta(\dot{\Delta}^* - im\Omega\Delta^*)] \right. \\ &\quad \left. + 2\Omega \mathcal{R}e(\mathcal{E}\Delta^*) \right\} , \end{aligned} \quad (33)$$

where $\mathcal{I}m(\dots)$ indicates the imaginary part. The radial flux-density of canonical angular momentum is

$$\mathcal{F}_{\mathcal{P}r} = \Sigma u^2 \mathcal{I}m[\mathcal{E}^* (ik_r \mathcal{E} - k_\phi \Delta)] , \quad (34)$$

from equation (26).

4.1 Mode Frequencies

Using equations (28) and taking $\mathcal{E}, \Delta \sim \exp(-i\omega t)$, we obtain

$$\begin{bmatrix} A_{11} & A_{12} \\ A_{21} & A_{22} \end{bmatrix} \begin{bmatrix} \mathcal{E} \\ \Delta \end{bmatrix} = 0 , \quad (35)$$

where

$$\begin{aligned} A_{11} &= -\tilde{\omega}^2 + 2\Omega r \Omega' + (k_r c_s)^2 - 2\pi G \Sigma k_r^2 / k , \\ A_{12} &= -2\Omega \tilde{\omega} + ik_r k_\phi c_s^2 - 2\pi i G \Sigma k_r k_\phi / k , \\ A_{21} &= -2\Omega \tilde{\omega} - ik_r k_\phi c_s^2 + 2\pi i G \Sigma k_r k_\phi / k , \\ A_{22} &= -\tilde{\omega}^2 + (k_\phi c_s)^2 - 2\pi G \Sigma k_\phi^2 / k , \end{aligned} \quad (36)$$

where $\tilde{\omega}(r) \equiv \omega - m\Omega(r)$ is the wave frequency in the reference frame comoving with the disk at r .

The dispersion relation implied by equation (35), $\det(A) = 0$, gives

$$\omega_{1,2,3,4} = m\Omega \pm_A \left\{ \frac{1}{2} \left[\kappa_r^2 + \mathbf{k}^2 u^2 \pm_B \sqrt{(\kappa_r^2 + \mathbf{k}^2 u^2)^2 - 8k_\phi^2 u^2 \Omega r \Omega'} \right] \right\}^{\frac{1}{2}} , \quad (37)$$

where the (A, B) subscripts on the \pm signs indicate that they are independent, and $\mathbf{k}^2 \equiv k_r^2 + k_\phi^2$. We adopt the convention that $\omega_\alpha(A, B) = \omega_1(+, +)$, $\omega_2(+, -)$, $\omega_3(-, +)$, and $\omega_4(-, -)$. The frequencies are invariant under $k_r \rightarrow -k_r$ owing to the time reversibility of the basic equations; trailing spiral waves ($k_r > 0$) are equivalent to leading waves ($k_r < 0$).

The mode frequencies found here differ in some respects from the standard analysis owing to our different application of the WKBJ approximation. In the standard approach, one takes, for example, $\nabla \cdot \delta \mathbf{v} \approx i\mathbf{k} \cdot \delta \mathbf{v}$ (Binney & Tremaine 1987, ch. 6; Kato *et al.* 1998, ch. 13), whereas we take $\nabla \cdot \boldsymbol{\xi} \approx i\mathbf{k} \cdot \boldsymbol{\xi}$. Note that the standard approach does not lead to equations of motion derivable from a Lagrangian.

For axisymmetric $k_\phi = m/r = 0$ perturbations, equation (37) gives two zero frequency modes and the two modes with

$$\omega = \pm \left(\kappa_r^2 + k_r^2 c_s^2 - 2\pi G \Sigma |k_r| \right)^{1/2} , \quad (38)$$

which is the same as the classical result of Toomre (1964) and Safronov (1960). As a function of k_r , ω^2 has a minimum at $k_{TS} = \pi G \Sigma / c_s^2$ at which point $\omega^2(k_{r0}) = \kappa_r^2 - (\pi G \Sigma / c_s)^2$. If this minimum value is less than zero, which occurs for $\Sigma > \Sigma_{TS} \equiv \kappa_r c_s / (\pi G)$, then one of the ω values is positive imaginary corresponding to a linear Jeans-type instability (Safronov 1960; Toomre 1964). With $Q \equiv \Sigma_{TS} / \Sigma$, there is instability for $Q < 1$ (Toomre 1964).

For tightly wrapped spiral waves ($k_r^2 \gg k_\phi^2$), the two modes with $\pm_B = +1$ simplify to $\omega = m\Omega \pm [\kappa_r^2 + k_r^2 c_s^2 - 2\pi G \Sigma |k_r|]^{1/2}$ which is the same as the dispersion relation of Lin and Shu (1966) and Kalnajs (1965) with the ‘‘reduction factor’’ $\mathcal{F} = 1$.

Consider now equation (37) for general (k_r, k_ϕ) with $|\mathbf{k}|$ increasing but with $\tan(\alpha) \equiv |k_\phi / k_r| = \text{const.}$ The argument of the inner square root in equation (37), $(\kappa_r^2 + \mathbf{k}^2 u^2)^2 - 8k_\phi^2 u^2 \Omega r \Omega'$, has a minimum as a function of $|\mathbf{k}|$ at $|\mathbf{k}| = k_{TS}$, the same as for $k_\phi = 0$. If the minimum of this argument is less than zero, one of the mode frequencies has a positive imaginary part (as well as a real part for $\omega - m\Omega$). This condition for instability can be expressed as

$$\frac{\Sigma_{crit}}{\Sigma_{TS}} > \left\{ 1 + \frac{2qS^2}{2-q} - 2 \left[\frac{qS^2}{2-q} + \frac{q^2 S^4}{(2-q)^2} \right]^{1/2} \right\}^{1/2}, \quad (39)$$

where $S \equiv \sin(\alpha) = |k_\phi| / |\mathbf{k}|$ and $q \equiv -d \ln \Omega / d \ln r$. For $S = 1$ this gives $\Sigma_{crit} / \Sigma_{TS} > 0.268$ (or $Q < 3.73$) for $q = 3/2$ and $\Sigma_{crit} / \Sigma_{TS} > 0.414$ (or $Q < 2.42$) for $q = 1$. Thus, the non-axisymmetric modes are unstable at larger Q than the axisymmetric modes.

For $|\mathbf{k}| > 2k_{TS}$, we have $\mathbf{k}^2 u^2 > 0$ so that the argument of the inner square root in equation (37) is greater than zero. As a result, the outer square root in equation (37) for $\pm_B = -1$ is purely imaginary if $q > 0$. Thus the mode with $\pm_A = +1$ is unstable for $q > 0$.

Figure 2 shows the four mode frequencies as a function of k_ϕ for a case with $\Sigma_{crit} < \Sigma < \Sigma_{TS}$.

4.2 Shearing of Unstable Modes with $k_\phi r \gg 1$

For an unstable wave with $k_\phi r = m \gg 1$, the geometrical optics relations for a wave-packet give

$$\frac{dk_r}{dt} = -\frac{\partial \omega}{\partial r} \approx q k_\phi \Omega, \quad \frac{d(rk_\phi)}{dt} = -\frac{\partial \omega}{\partial \phi} = 0, \quad (40)$$

so that $k_r \approx q k_\phi \Omega t + \text{const.}$, and $r k_\phi = \text{const.}$ Thus, a wave-packet initially with long radial wavelength, with $|k_r| h \ll 1$, is rapidly sheared by the differential rotation of the disk if $q > 0$. In a time of order $t_{shear} = (q k_\phi h \Omega)^{-1}$ the wave evolves into a very short radial wavelength, $|k_r| h \gtrsim 1$, trailing spiral wave. This is discussed in detail by Goldreich and Lynden-Bell (1965). The maximum amplification a wave can have (without reflections) is $A = \exp(\int dt \omega_i) \sim$

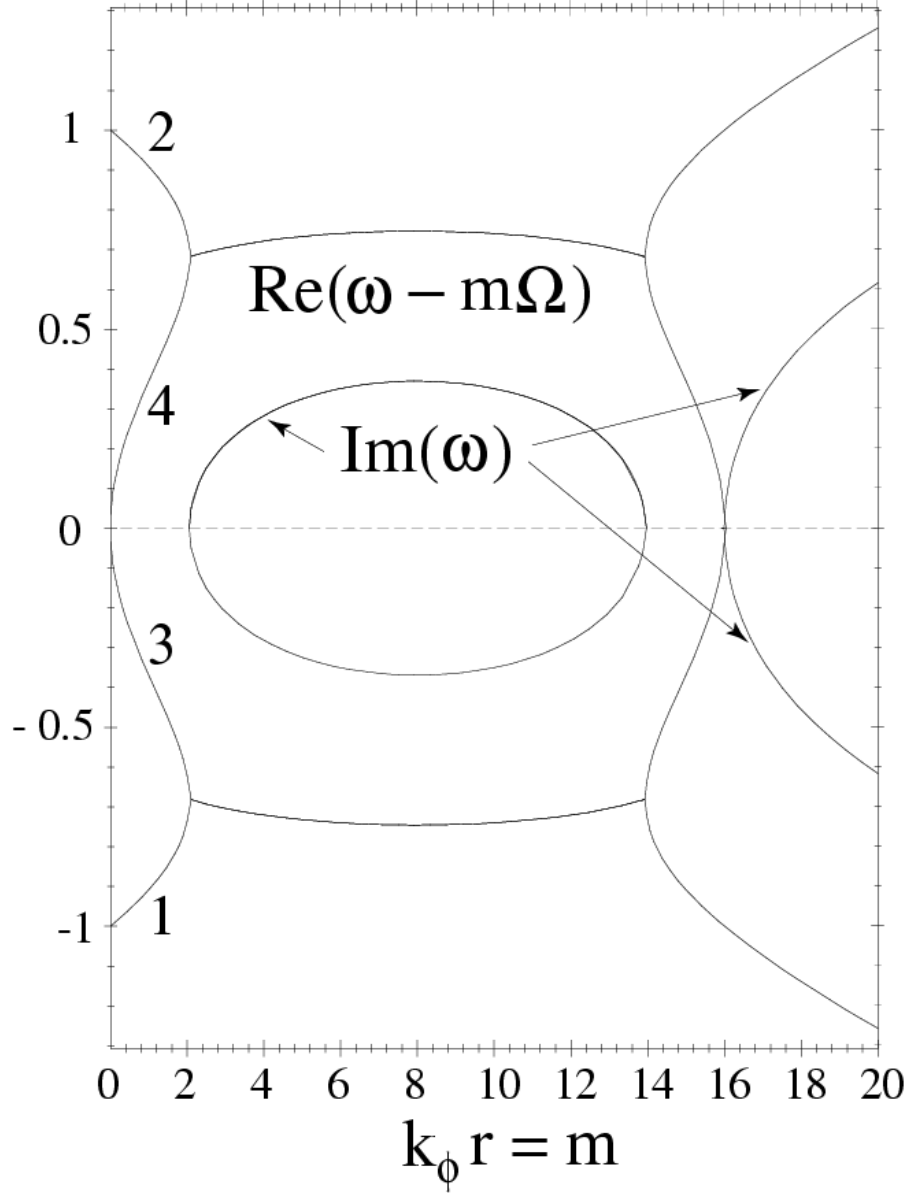


Figure 2: Real and imaginary parts of the four mode frequencies (labeled 1, ..., 4) normalized by Ω for $k_\phi^2 \gg k_r^2$, $c_s/(r\Omega) = 0.05$, and $\Sigma = 0.4\Sigma_{TS}$, where Σ_{TS} is the surface density at which the Toomre-Safronov instability sets in for axisymmetric perturbations. We have taken $q = 3/2$ which corresponds to a Keplerian disk. For these conditions $rk_{TS} = 8$.

$\exp[\max(\omega_i)t_{shear}]$, where $\omega_i = \mathcal{I}m(\omega)$ is the growth rate. For the above-mentioned unstable modes for $\Sigma_{crit} < \Sigma < \Sigma_{TS}$, which have $k_\phi r \gg 1$, we find $A \sim \exp(1)$, which is probably not significant in the absence of reflections or trapping of the waves in the vicinity of a bump in the disk as a function of r (Lovelace *et al.* 1999a; Li *et al.* 2000).

5 Negative Energy Modes

We consider the case of a low mass disk around a Schwarzschild black hole where the inner radius of the disk is at $r_i = 3r_S$ with $r_S \equiv 2GM/c^2$ the Schwarzschild radius. We adopt the pseudo-Newtonian potential $\Phi = -GM/(r-r_S)$ (Paczynski & Wiita 1980; Kato *et al.* 1998, ch. 2). For this potential,

$$\Omega = \left(\frac{GM}{r(r-r_S)^2} \right)^{1/2}, \quad \frac{\kappa_r}{\Omega} = \left(\frac{r-3r_S}{r-r_S} \right)^{1/2},$$

$$q \equiv -\frac{d \ln \Omega}{d \ln r} = \frac{3}{2} \frac{r-r_S/3}{r-r_S}. \quad (41)$$

Figure 3 shows the radial variations of these quantities near the inner edge of the disk. In the following the mode frequency ω is measured in units of $\Omega_S \equiv \sqrt{GM/r_S^3}$, while Ω is in units of s^{-1} . Radial distance R and $1/k_r$ are measured in units of r_S , while \mathcal{E} and Δ are in units of length. Note that $\Omega_S \approx 7.16 \times 10^4 (M_\odot/M) s^{-1}$ and $r_S \approx 2.96 \times 10^5 (M/M_\odot) \text{cm}$.

5.1 One-Armed Spiral Waves ($m = 1$)

Figure 4 shows the radial wavenumber dependence of the low-frequency mode ω_1 and the corresponding mode energy (per unit area) dE/dA (from equation (31)) for a sample case for $k_r \geq 0$ which corresponds to a *trailing* spiral wave. (The 1-subscript on ω is dropped in the following.) The radial phase velocity is outward ($\omega/k_r > 0$) and the azimuthal phase velocity is positive ($\omega r > 0$). [Note that both quantities plotted in Figure 4 are even functions of k_r , so that the plot is the same for $k_r < 0$ which corresponds to a leading spiral wave.] For k_r less than a certain value k_{r0} , the wave frequency is positive while the wave energy is *negative*. Further, the energy flux-density of the perturbation \mathcal{F}_{Er} (from equation (32)) is positive (outward) for $k_r < k_{r0}$ and negative for $k_r > k_{r0}$.

From Figure 4 the group velocity $v_{gr} = \partial\omega/\partial k_r$ is negative for $k_r > 0$. Thus, the sign of $\mathcal{F}_{Er}/(dE/dA) < 0$ is the same as that of v_{gr} for $k_r \lesseqgtr k_{r0}$ as it should be. Note that the radial phase and group velocities have opposite signs.

The canonical angular momentum (per unit area) \mathcal{P}_ϕ (from equation 33) is negative and the flux of angular momentum $\mathcal{F}_{\mathcal{P}r}$ (from equation 34) is positive for the low frequency mode for $k_r \lesseqgtr k_{r0}$. Thus $\mathcal{F}_{\mathcal{P}r}/\mathcal{P}_\phi < 0$ has the same sign as v_{gr} .

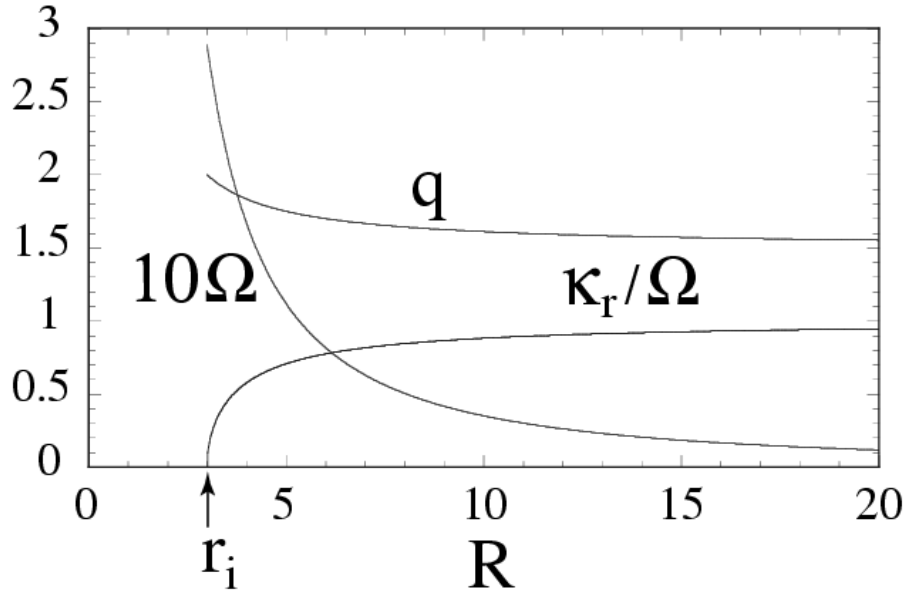


Figure 3: Radial variations of equilibrium disk quantities of equation (41) with $R \equiv r/r_S$ and Ω measured in units of $\Omega_S \equiv (GM/r_S^3)^{1/2}$.

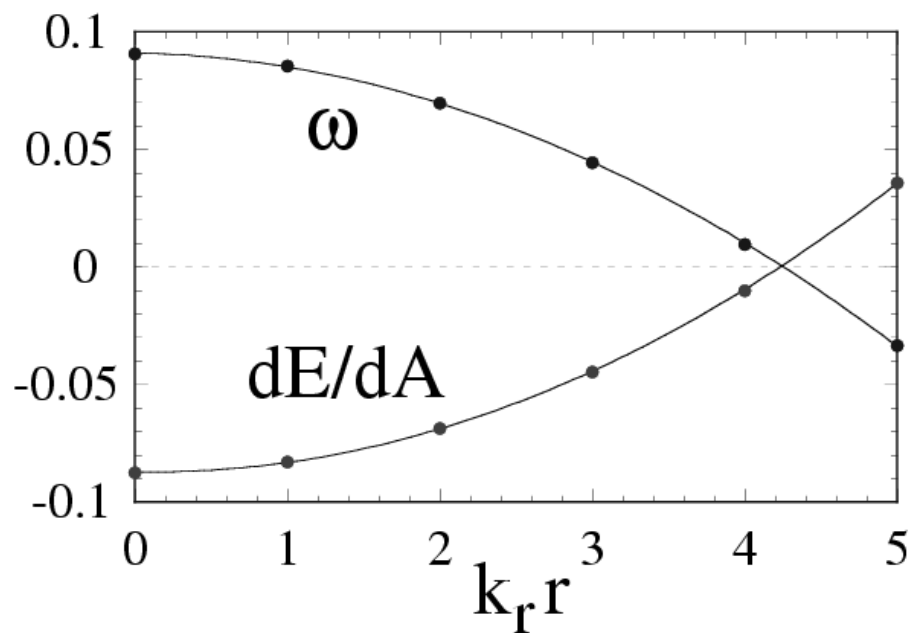


Figure 4: Dependence of the low-frequency mode ω on radial wavenumber from equation (37) and the corresponding wave energy (per unit area) dE/dA from equation (31). For $k_r < 0$ note that both curves are even functions of k_r . Here, ω is normalized by Ω_S , and dE/dA by $\Sigma\Omega^2|\mathcal{E}|^2/2$. For this plot $R = 10$ and $c_s/(r\Omega) = 0.1$.

Table 1: Physical Quantities for the Low-Frequency Mode

	ω	dE/dA	\mathcal{F}_{Er}	$v_{gr} = \partial\omega/\partial k_r$	\mathcal{P}_ϕ	$\mathcal{F}_{\mathcal{P}r}$
$0 < k_r < k_{r0}$	+	-	+	-	-	+
$k_r > k_{r0}$	-	+	-	-	-	+

The signs of the different quantities are summarized in Table 1 for the trailing waves ($k_r > 0$). For the leading waves, $k_r \rightarrow -k_r$, the signs of dE/dA and \mathcal{P}_ϕ do not change, but the signs of the fluxes \mathcal{F}_{Er} and $\mathcal{F}_{\mathcal{P}r}$ reverse as does the sign of the group velocity v_{gr} .

In contrast, for the high-frequency mode ω_2 , the wave energy is *positive* independent of k_r . Also, the angular momentum \mathcal{P}_ϕ is positive.

For the low-frequency mode the approximate dependence is

$$\omega = \omega_0 \left(1 - \frac{(k_r r)^2}{(k_r r)_0^2} \right) . \quad (42)$$

Figure 5 shows the R -dependences of ω_0 and $(k_r r)_0$ for $c_s/(r\Omega) = 0.1$. For this case $\omega_0 \approx C_\omega/R^a$ with $C_\omega = 4.71$, $a = 3.16$ and $(k_r r)_0 \approx C_k/R^b$ with $C_k = 21.1$, $b = 0.702$. The frequency is of course independent of R so that

$$k_r^2 = \frac{C_k^2}{R^{2+2b}} \left(1 - \frac{\omega R^a}{C_\omega} \right) , \quad (43)$$

where the allowed region $k_r^2 \geq 0$ extends from the inner radius of the disk $R = R_i = 3$ out to the turning point $R_{turn} = (C_\omega/\omega)^{1/a} > 3$.

Because $dE/dA \approx -\omega\Sigma\Omega^2|\mathcal{E}|^2/2$, we have

$$E \approx -\pi r_S^2 \omega \int_{R_i}^{\infty} R dR \Sigma \Omega^2 |\mathcal{E}|^2 , \quad (44)$$

which is negative in that $\omega > 0$ for the ‘bound states’. Also, we find $\mathcal{P}_\phi \approx -\Sigma\Omega|\mathcal{E}|^2$ so that the total canonical angular momentum of the disk perturbations is

$$L_z \approx -\pi r_S^2 \int_{R_i}^{\infty} R dR \Sigma \Omega |\mathcal{E}|^2 . \quad (45)$$

We discuss the mode energy and angular momentum further in §5.3.

In the limit $\omega \rightarrow 0$, the trailing spiral wave for example has the form $R = R_i/(1 + b3^b\phi/C_k)^{1/b}$ for $\phi \leq 0$.

5.2 Standing Waves

A standing wave solution for say \mathcal{E} can be written as

$$\begin{aligned} \mathcal{E} &= \mathcal{E}_+ + \mathcal{E}_- , \\ &= A|k_r|^{-1/2} \exp(i\Psi) + B|k_r|^{-1/2} \exp(-i\Psi) , \end{aligned} \quad (46)$$

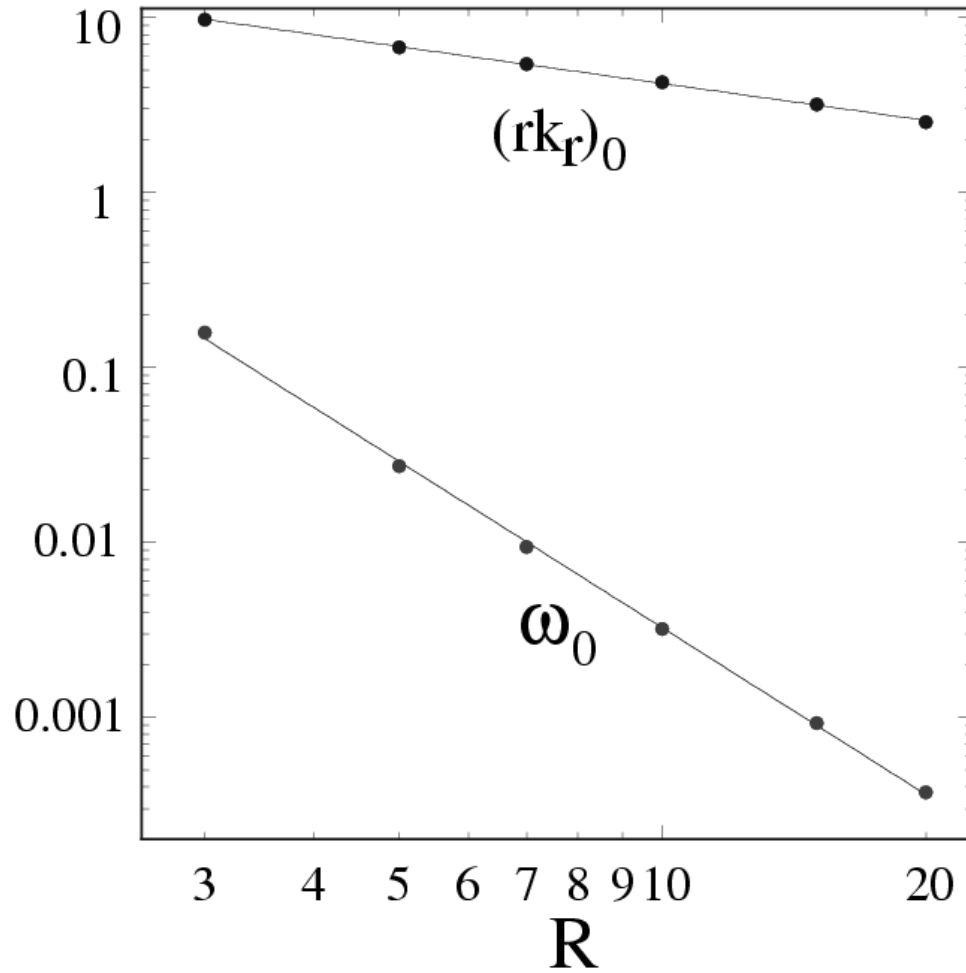


Figure 5: Radial dependences of the two ‘constants’ in equation (42) for the case where $c_s/(r\Omega) = 0.1$. The straight lines correspond to least squares fits through the shown points which give $(k_r r)_0 = 21.1/R^{0.702}$ and $\omega_0 = 4.71/R^{3.16}$.

where the \mathcal{E}_+ term corresponds to a trailing spiral wave and the \mathcal{E}_- term a leading wave. Also,

$$\Psi(R, \omega) \equiv \int_{R_i}^R dR' k_r(R', \omega) \quad (47)$$

is the phase with the ω dependence made explicit. An expression for Δ in terms of \mathcal{E} can be derived from equations (35) and (36).

The specific nature of the modes clearly requires a definite boundary condition at the inner edge of the disk. The present model, which neglects v_r , does not allow a full treatment of the inner radius of the disk where the radial inflow may be transonic (see for example Kato *et al.* 1998, ch. 9). Instead, we first consider an inner disk boundary condition appropriate for the Shakura and Sunyaev (1973) model where for $r \rightarrow r_i$, $\Sigma \rightarrow \infty$; namely, $\mathcal{E}(r_i = 3r_S) = 0$, which corresponds to perfect reflection. For this boundary condition, and the usual WKBJ matching at the outer turning point R_{turn} , we obtain the Bohr-Sommerfeld quantization condition

$$\Psi(R_{turn}, \omega) = \left(n + \frac{3}{4} \right) \pi, \quad n = 0, 1, 2, \dots, \quad (48)$$

which determines the allowed ω values. The $3/4$ in equation (48) (rather than $1/2$) is due to the boundary condition at R_i . For the mentioned dependences of ω_0 and $(k_r r)_0$, and $c_s/(r\Omega) = \text{const}$, there are a finite number of modes n with the lowest frequency corresponding to the largest n value.

Instead of using the approximate equation (48), we solve the wave equation for the perturbation amplitude,

$$\frac{d^2 \mathcal{E}}{dR^2} = -k_r^2(R, \omega) \mathcal{E}. \quad (49)$$

This is done using a shooting method: We guess ω , integrate outward from $R = R_i = 3$, and require $\mathcal{E}(R \rightarrow \infty) \rightarrow 0$. This requirement determines the allowed frequency values. Figure 6 shows the behavior of the wave functions for a sample case with $c_s/(r\Omega) = 0.1$. The corresponding frequencies in units of Ω_S are $\omega_n \approx 3.75 \times 10^{-2}$, 7.74×10^{-3} , and 8.69×10^{-4} for $n = 0, 1, 2$, respectively. For a $M = 10M_\odot$ black hole, these frequencies in Hz are: 268, 55.4, and 6.22. These frequencies agree approximately with those obtained from equation (48). This equation implies that there are only three modes (or bound states) for $c_s/(r\Omega) = 0.1$.

Figure 7 shows the variation of the mode frequencies with the disk thermal speed $c_s/(r\Omega)$.

With regard to the energy of the standing wave modes, notice that we now have in place of equations (28) separate equations for \mathcal{E}_+ , \mathcal{E}_- , Δ_+ , and Δ_- . Thus the Lagrangian density becomes $\mathcal{L} = \mathcal{L}_+(\mathcal{E}_+, \dots) + \mathcal{L}_-(\mathcal{E}_-, \dots)$, and the Hamiltonian $\mathcal{H} = \mathcal{H}_+ + \mathcal{H}_-$. The energy of the trailing and leading components are equal and negative. Thus the total energy $E = E_+ + E_-$ is negative. From

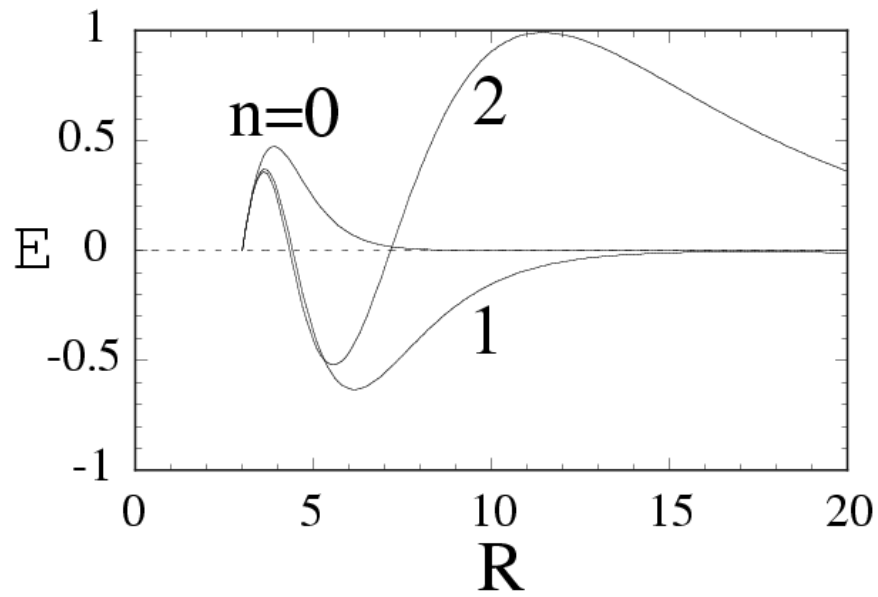


Figure 6: Wave function profiles $\mathcal{E}_n(R)$ for the three low-frequency standing wave modes for the case $c_s/(r\Omega) = 0.1$ obtained by solving equation (49) using a shooting method. The normalization of the different wavefunctions results from the boundary condition $(d\mathcal{E}_n/dR)_i = 1$.

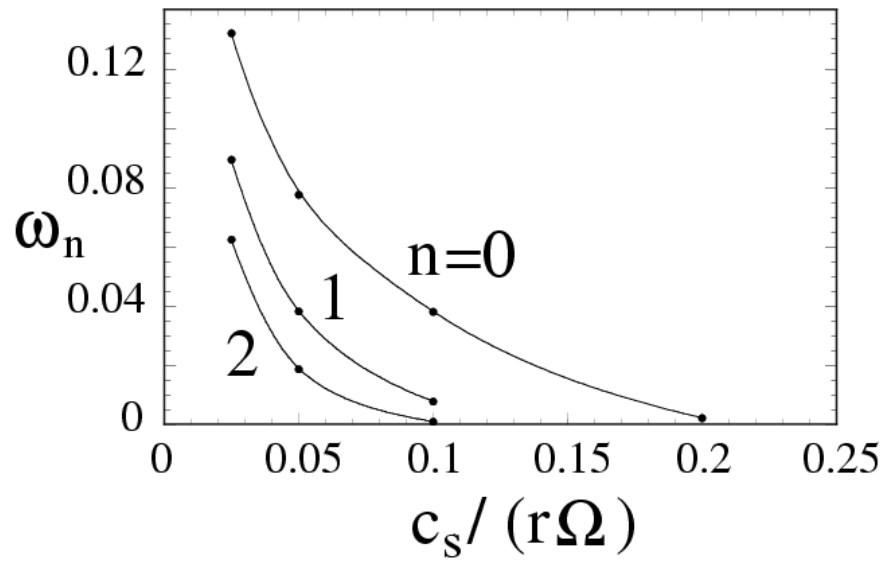


Figure 7: Dependence of mode frequencies ω_n in units of Ω_S on the disk temperature as measured by $c_s/(r\Omega)$. The curves are smooth fits through the shown points.

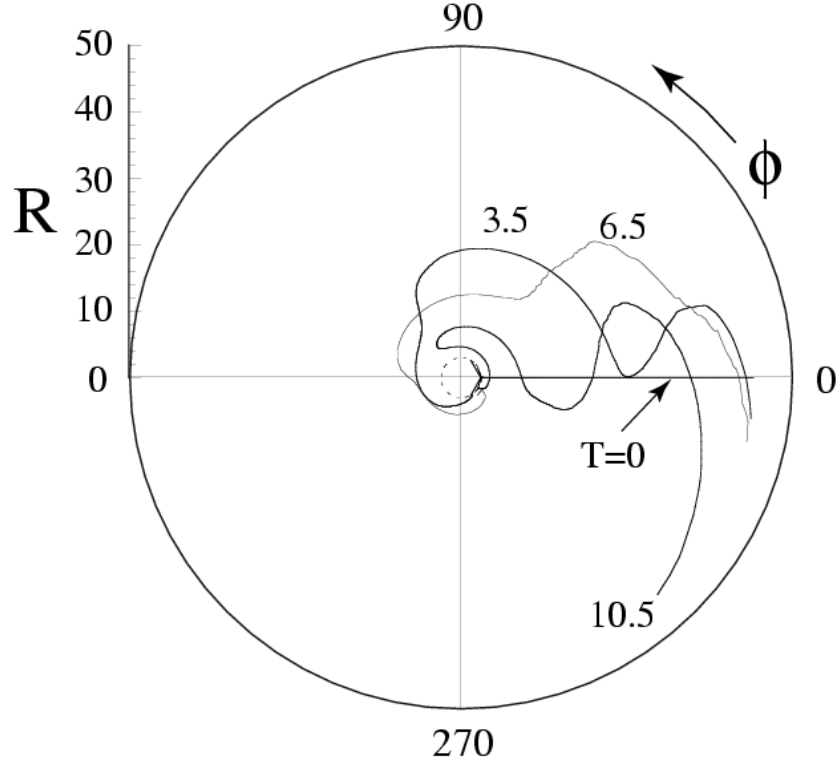


Figure 8: Time dependence of the line-of-nodes angle $\varphi(R, T)$, which is such that $\mathcal{E} = |\mathcal{E}(R, T)| \exp[-i\varphi(R, T)]$, obtained by solving the Schrödinger equation (51) for an initial wavefunction $\mathcal{E}(R, T = 0) = \text{const}(R - 3) \exp(-R/4)$ which is *not* an eigenfunction. The boundary conditions were $\mathcal{E}(R_i) = 0 = \mathcal{E}(R_{max})$ and a nonuniform mesh $R_j = R_i Q^j$, $j = 1, \dots, 300$ with $Q = 1.009$ so that $R_{max} \approx 44.1$. The time-dependent evolution represents a superposition of the three eigenfunctions shown in Figure 6 with the average of the energy $\langle \tilde{E} \rangle = -8.09 \times 10^{-3}w$. The plot shows the reflection of a trailing spiral wave ($T \lesssim 125$) from the inner disk radius which gives rise to a leading spiral wave ($T \gtrsim 125$) for $3 \leq R \lesssim 5.6$.

equation (32) the total energy flux is

$$\begin{aligned}
\mathcal{F}_{Er} &= \omega \Sigma c_s^2 \mathcal{I}m \left(\mathcal{E}_+^* \frac{\partial \mathcal{E}_+}{\partial R} + \mathcal{E}_-^* \frac{\partial \mathcal{E}_-}{\partial R} \right) , \\
&= \omega \Sigma c_s^2 \mathcal{I}m \left(\mathcal{E}^* \frac{\partial \mathcal{E}}{\partial R} \right) , \\
&= \omega \Sigma c_s^2 |k_r| (|\mathcal{E}_+|^2 - |\mathcal{E}_-|^2) .
\end{aligned} \tag{50}$$

For the considered boundary condition at the inner disk radius $R = 3$, $\mathcal{F}_{Er} = 0$. At large distances, $\mathcal{F}_{Er} = 0$ because $\mathcal{E}(R \rightarrow \infty) = 0$. Thus from equation (21) we have $dE/dt = 2\pi(r\mathcal{F}_{Er})_i - 2\pi(r\mathcal{F}_{Er})_\infty = 0$, where the i -subscript indicates evaluation at $R = 3$. Similar conclusions apply to the canonical angular momentum where $\mathcal{F}_{Pr} = \Sigma c_s^2 |k_r| (|\mathcal{E}_+|^2 - |\mathcal{E}_-|^2)$.

5.3 Time-Dependent Solutions

Equation (49) can be written in the form of a Schrödinger equation

$$\frac{w}{i} \frac{\partial \mathcal{E}}{\partial T} = \left[-\frac{\partial^2}{\partial R^2} + U(R) \right] \mathcal{E} , \tag{51}$$

where $T \equiv \Omega_S t$, $U(R) \equiv -C_k^2/R^{2+2b}$ and $w \equiv (C_k^2/C_\omega)/R^{2+2b-a}$. The R -dependence of w is rather weak ($\sim R^{-0.24}$ for $c_s/(r\Omega) = 0.1$) and for this reason we make the simplification that $w = w(R = R_i)$. The sign of the time derivative is opposite that of Schrödinger equation because the energy is negative for $\omega > 0$.

For the mentioned bound states, $\tilde{E}_n = -w\omega_n$, where the tilde indicates a different normalization of the energy compared with equation (44). For the unbound states or continuum modes we have $\omega_k < 0$ and $\tilde{E}_k = -w\omega_k > 0$. For the continuum trailing waves ($k_r > 0$) both the radial phase and group velocities are negative, whereas for the leading waves ($k_r < 0$) both are positive.

Figure 8 shows polar plot (see Briggs 1990; LZKH) of the time-dependence of the mode for an assumed initial perturbation $\mathcal{E}(R, T = 0) = \text{const}(R - R_i) \exp(-R/4)$ which is neither leading nor trailing. The mode evolves to a predominantly *trailing spiral wave*. Trailing spiral one-armed spiral waves were found under different conditions in our earlier study of galactic disks (LZKH).

6 Conclusions

The perturbations of thin disks have been studied in many works applied to understanding the waves or modes in galactic disks and in accretion disks. This work has derived the linearized equations of motion, the Lagrangian density, the Hamiltonian density, and the canonical angular momentum density for general perturbations [$\propto \exp(im\phi)$ with $m = 0, \pm 1, \dots$] of a geometrically thin self-gravitating, homentropic fluid disk including the pressure. The theory was applied to the ‘‘eccentric,’’ $m = \pm 1$ perturbations of a geometrically thin Keplerian

disk. The $m = 1$ modes may be at low frequencies compared to the Keplerian frequency. Furthermore, the modes can have negative energy and negative angular momentum. Their propagation can remove angular momentum from the inner region of a disk and thus act to enhance the accretion of matter. Dependent on the radial boundary conditions, there are discrete, low-frequency, negative energy $m = 1$ modes. Time-dependent perturbations tend to give rise to predominantly trailing spiral waves. A future direction for extending this paper include the treatment of the non-linear evolution following the approach of Shu, Yuan, and Lissauer (1985), Heemskerk, Papaloizou, and Savonije (1992), and Lee and Goodman (1999).

We thank M.P. Haynes, D.A. Kornreich, N.F. Comins, and M.M. Romanova for stimulating discussions on eccentric perturbations of disks. This work was supported in part by NASA grants NAGS-9047, NAGS 9735, by NSF grant AST-9986936, and by CRDF grant KP-2555-AL-03.

References

- [1] Adams, F. C., Ruden, S. P., & Shu, F. H. 1989, *ApJ*, 347, 959
- [2] Andersson, N. 1998, *ApJ*, 502, 708
- [3] Baldwin, J.E., Lynden-Bell, D., & Sancisi, R. 1980, *MNRAS*, 193, 313
- [4] Binney, J., & Tremaine, S. 1987, *Galactic Dynamics* (Princeton: Princeton University Press)
- [5] Briggs, F.H. 1990, *ApJ*, 352, 15
- [6] Coppi, B., Rosenbluth, M.N., & Sudan, R.N. 1969, *Ann. of Physics*, 55, 207
- [7] Fridman, A.M., Boyarchuk, A.A., Bisikalo, D.V., Kuznetsov, O.A., Khorushii, O.V., Torgashin, Yu.M., & Kilpio, A.A. 2003, *Physics Letters A*, 317, 181
- [8] Frieman, E., & Rotenberg, M. 1960, *Rev. Mod. Phys.*, 32, 898
- [9] Goldreich, P., & Lynden-Bell, D. 1965, *MNRAS*, 130, 125
- [10] Goldstein, H. 1950, *Classical Mechanics* (Addison-Wesley: Cambridge, Massachusetts)
- [11] Goodman, J., Narayan, R., & Goldreich, P. 1987, *MNRAS*, 225, 695
- [12] Heemskerk, M. H. M., Papaloizou, J. C., & Savonije, G. J. 1992, *A&A*, 260, 161
- [13] Kalnajs, A.J. 1965, Ph.D. thesis, Harvard University

- [14] Kato, S., Fukue, J., & Mineshige, S. 1998, *Black-Hole Accretion Disks* (Kyoto University Press: Kyoto, Japan)
- [15] Kornreich, D.A., Haynes, M.P., & Lovelace, R.V.E. 1998, AJ, 116, 2154
- [16] Kornreich, D.A., Lovelace, R.V.E., & Haynes, M.P. 2002, ApJ, 580, 705
- [17] Lee, E., & Goodman, J. 1999, MNRAS, 308, 984
- [18] Li, H., Finn, J.M., Lovelace, R.V.E., & Colgate, S.A. 2000, ApJ, 533, 1023
- [19] Lin, C.C., & Shu, F.H. 1966, Proc. Nat. Acad. Sci., 55, 229
- [20] Lovelace, R.V.E. 1998, A&A, 338, 819
- [21] Lovelace, R.V.E., Li, H., Colgate, S.A., & Nelson, A.F. 1999a, ApJ, 513, 805
- [22] Lovelace, R.V.E., Zhang, L., Kornreich, D.A., & Haynes, M.P. 1999b, ApJ, 524, 634
- [23] Lynden-Bell, & Ostriker, J.P. 1967, MNRAS, 136, 293
- [24] Nowak, M.A., & Wagoner, R.V. 1991, ApJ, 378, 656
- [25] Nowak, M.A., & Wagoner, R.V. 1992, ApJ, 393, 697
- [26] Paczyński, B., & Wiita, P.J. 1980, A&A, 88, 23
- [27] Rix, H.-W., & Zaritsky, D. 1995, ApJ, 447, 82
- [28] Safronov, V.S. 1960, Ann. Astrophys., 23, 982
- [29] Shakura, N.I., & Sunyaev, R.A. 1973, A&A, 24, 337
- [30] Schenk, A. K., Arras, P., Flanagan, É. É., Teukolsky, S. A., & Wasserman, I. 2002, Phys. Rev. D, 65, 024001
- [31] Shu, F. H., Yuan, C., & Lissauer, J. J. 1985, ApJ, 291, 356
- [32] Shu, F. H., Tremaine, S., Adams, F. C., & Ruden, S. P. 1990, ApJ, 358, 495
- [33] Toomre, A. 1964, ApJ, 139, 1217
- [34] Tremaine, S. 2001, AJ, 121, 1776
- [35] van der Klis, M. 2000, Ann. Rev. of Astron. and Astrophysics, 38, 717
- [36] Zeltwanger, T., Comins, N.F., & Lovelace, R.V.E. 2000, ApJ, 543, 669